REPORT DOCUMENTATION PAGE

Form Approved OMB No. 0704-0188

1. REPORT DATE *(DD-MM-YYYY)*	2. REPORT TYPE	3. DATES COVERED *(From – To)*
27-01-2009	Final Report	15 November 2006 - 28-Jan-10

4. TITLE AND SUBTITLE

Study of the influence of the chemical bond on the glass forming ability of amorphous alloys by X-ray absorption spectroscopy (XANES)

5a. CONTRACT NUMBER
FA8655-07-M-4003

5b. GRANT NUMBER

5c. PROGRAM ELEMENT NUMBER

6. AUTHOR(S)

Dr. Stéphane B Gorsse

5d. PROJECT NUMBER

5d. TASK NUMBER

5e. WORK UNIT NUMBER

7. PERFORMING ORGANIZATION NAME(S) AND ADDRESS(ES)

ICMCB-CNRS
87, Avenue du Docteur Schweitzer
PESSAC 33608
France

8. PERFORMING ORGANIZATION REPORT NUMBER

N/A

9. SPONSORING/MONITORING AGENCY NAME(S) AND ADDRESS(ES)

EOARD
Unit 4515 BOX 14
APO AE 09421

10. SPONSOR/MONITOR'S ACRONYM(S)

11. SPONSOR/MONITOR'S REPORT NUMBER(S)
SPC 07-4003

12. DISTRIBUTION/AVAILABILITY STATEMENT

Approved for public release; distribution is unlimited. (approval given by local Public Affairs Office)

13. SUPPLEMENTARY NOTES

14. ABSTRACT

This report results from a contract tasking ICMCB-CNRS as follows: One of the most appropriate techniques to study the structural features of amorphous materials and to characterize the electronic structure (chemical bond) is X-ray absorption spectroscopy near edge structure (XANES).
Synchrotron radiation will be used to analyze the influence of the solutes on the XANES spectra of Zr-based metallic glasses. Quantum calculations based on the FLAPW (full potential linearized augmented plane wave) ab initio codes will be exploited for a quantitative analysis and calculation of the XANES spectra. Zr-based metallic glasses are of interest because they have good mechanical properties. This study will focus on Zr-Al-X glass forming systems, with X = Cu, Ni, Co or Fe, because they are topologically equivalent (since Ni, Cu, Co and Fe all have essentially identical radii), but exhibit very different glass forming abilities. Zr-Al-Ni is by far the best of these systems, and Zr-Al-(Cu,Ni) is much better than either Zr-Al-Ni or Zr-Al-Cu. The influence of chemical bonding is the likely explanation for these different behaviours in topologically equivalent glasses. A series of Zr-based bulk metallic glasses (Zr-Al-Cu, Zr-Al-Ni, Zr-Al-Cu-Ni) will be characterized by X(ray absorption spectroscopy and PPMS (Physical Properties Measurement System) in order to study the influence of the solute atom, X (with X = Cu, Ni), on the local order (atomic distances, nature and number of neighbour atoms), oxidation states, electronic structures and heat capacity.

15. SUBJECT TERMS
EOARD, Bulk Amorphous Metals

16. SECURITY CLASSIFICATION OF:			17. LIMITATION OF ABSTRACT	18, NUMBER OF PAGES	19a. NAME OF RESPONSIBLE PERSON
a. REPORT	b. ABSTRACT	c. THIS PAGE			WYNN SANDERS, Maj, USAF
UNCLAS	UNCLAS	UNCLAS	UL	20	19b. TELEPHONE NUMBER *(Include area code)* +44 (0)1895 616 007

December 20th 2008

Study of the influence of the chemical bond on the glass forming ability of amorphous alloys

---

EOARD Contract N°: FA8655-07-M-4003

Final Report

Al/Ni/Zr and Al/Cu/Zr glass forming systems: a first-principles comparative study of chemical bonding and cohesive energies

by A. Villesuzanne
&
S. Gorsse
gorsse@icmcb-bordeaux.cnrs.fr

Institut de Chimie de la Matière Condensée de Bordeaux
ICMCB - CNRS – 87, Av du Dr Schweitzer – 33608 PESSAC Cedex (France)
www.icmcb-bordeaux.cnrs.fr

Goal of the project:

To establish an understanding of the roles of chemistry on metallic glass stability through first-principles calculations.

Table of contents

1. Introduction

It has long been known that chemistry and topology are both important in the glass forming ability of metallic melt. The primacy of these features are reflected in 2 of the 3 phenomenological rules [1] for formation of bulk metallic glasses (BMGs)- a large atomic size mismatch (topology) and a large negative enthalpy of mixing (chemistry). While these rules are rather general, recent results now provide specific information regarding the way in which topology establishes structure. The efficient cluster packing (ECP) model [2,3] establishes representative local and medium-range structure building from the principle of efficient atomic packing. Topology is given by the particular sizes and concentrations of constituent atoms in the metallic glass.

While the ECP model describes how topology produces structure, it cannot yet predict stability, in part because explicit chemical contributions are lacking. If structure alone influences stability, then topologically identical structures might be expected to have similar stabilities. However, it is well-known that metallic glass stability in a given alloy can be dramatically altered through atom-for-atom substitution of same-sized atoms.

The complementary roles of topology and chemistry on glass forming ability can be studied by careful selection of metallic glasses that are topologically identical but chemically distinct. The purpose of this work is to conduct such a study. Two related series of glasses will be studied; the topological binary $Zr_X(Cu,Ni)_Y$ series and the topological ternary $Zr_AAl_B(Cu,Ni)_C$ series of glasses. The Zr-Al-(Ni,Cu) system is chosen for study, as it represents the most widely studied BMG system. Zr-Ni and Zr-Cu both form binary glasses with solute concentrations in the range of 30-50% [4]. While Zr-Al does not form a binary glass, small Al additions to Zr-Ni or Zr-Cu dramatically improve stability [5]. The influence of chemistry (Al substitution) on stability is analyzed in terms of chemical bonding and electronic structure.

A structural model is a prerequisite for a first-principles study of electronic structure and chemical bonding. Either experimental or calculated (molecular dynamics) structures can be used as input; here, we chose to start with the experimentally determined crystal structures for $CuZr_2$ and $NiZr_2$, that can be considered as parent structures of the glasses. These compounds have the appropriate stoichiometry for extrapolation to some glasses under study, and their crystal structure allows the calculations for extended (periodic) systems, without artificial boundary effects. The Al:metal substitution can be easily simulated, and a comparative study of the Zr-Cu- and Zr-Ni systems, with or without substitution by Al, was

achieved. The effects of the Al:metal substitution was also carefully investigated within each system.

2. Structural models

The experimental crystal structures for $CuZr_2$ and $NiZr_2$ were used as input for our calculations. Al:Cu and Al:Ni substitutions in $CuZr_2$ and $NiZr_2$ were simulated by using multiple cells (2×2×2 and 1×1×2, respectively), in order to achieve the formulations $AlCu_3Zr_8$ and $AlNi_3Zr_8$, which are within the glass forming composition range.

In $CuZr_2$ with tetragonal structure [6] (space group I4/mmm, 2 formula unit (FU) per cell), Cu atoms lie in a Zr_8 cubic regular site ($d_{Cu\text{-}Zr}$ = 2.848 Å) and each Zr atom has four Cu first neighbors and four Zr atoms as second neighbors ($d_{Zr\text{-}Zr}$ = 3.140 Å). The crystal structure for $NiZr_2$ is quite different [7] (Al_2Cu structure type, space group I4/mcm, 4 formula unit per cell); Ni atoms lie in flattened and twinned Zr_8 cubic site ($d_{Ni\text{-}Zr}$ = 2.761 Å) and form 1D chains along the *c* axis, with short metal-metal distances ($d_{Ni\text{-}Ni}$ = 2.634 Å); Zr atoms have four Ni first neighbors and three Zr neighbors in a second coordination shell ($d_{Zr\text{-}Zr}$ = 2.989 Å ×1, 3.079 Å × 2).

3. Computational details

Density functional theory calculations were performed using the augmented plane wave plus local orbitals method (APW+lo, as implemented in the WIEN2k code [8-10]) and the generalized gradient approximation for the exchange-correlation potential, according to the formulation by Perdew, Burke and Ernzerhof (PBE).[11] Muffin-tin radii were chosen as 2.50 a.u. for Zr and Cu, and 2.49 a.u. for Ni. 1000 k-points were used for sampling the first Brillouin zone. In the case of 2×2×2 and 1×1×2 multiple cells, 100 and 500 k-points samplings were used, respectively.

Formation enthalpies were calculated by subtracting the total energies for elemental Al (fcc, *a* = 4.050 Å), Cu (fcc, *a* = 3.6144 Å), Ni (fcc, *a* = 3.5236 Å, ferromagnetic) and Zr (hcp, *a* = 3.233 Å, *c* = 5.1475 Å) metals from the compound total energy, according to the stoichiometry. Special care was taken for calculating all energies at the same approximation level (APW + lo / PBE), and with identical (or closest possible) numerical parameters (muffin-tin radii, cutoff energies …). In all calculations for elemental metals, both spi-

polarized and non spin-polarized solutions were calculated, to ensure that the calculated ground state has the correct magnetization (actually, only Ni is found ferromagnetic).

The topologic analysis of the calculated electron density was performed using R. F. W. Bader's "Atoms in Molecules" (AIM) theory,[12-15] as implemented in the WIEN2k code. The AIM method relies on a non-ambiguous definition of atomic boundaries: atomic frontiers are defined as surfaces of zero-flux in the gradient vectors of electron density (i.e. ensemble of density local minima along directions passing through the nuclei). The overall electron density is thus partitioned in well-defined atomic basins, with no interstitial space left. The atomic charges are then calculated by integration of the electron density in atomic basins. The AIM method constitutes a sophisticated tool for the characterization of chemical bonding, by the analysis of features at critical points of the electron density. This approach will be detailed in Part 4.3.

4. Results.

4.1. Formation enthalpies

Table 1 lists the energies calculated from DFT for elemental metals and the compounds under study. The formation energies deduced for $CuZr_2$ and $NiZr_2$ are in very good agreement with experimental values [16,17] (-45.09 to -49.78 kJ/mol and -95.24 kJ/mol, respectively). This is a key point for checking the reliability of DFT calculations for formation energies in these compounds, before the examination of substitution effects.

Al:Cu and Al:Ni 25% substitution in $CuZr_2$ and $NiZr_2$ induces a slight destabilization in the case of $CuZr_2$ (+1.3 kJ/mol, i.e. 3%) and a significantly larger one in $NiZr_2$ (+16.7 kJ/mol, i.e. 17%). This might been due, at least partly, to the perturbation of strong Ni-Ni interactions by the Al:Ni substitution in Ni infinite chains along the *c* axis.

Table1. Total electronic energies per formula unit (FU) for elemental metals, MZr_2 (M = Cu, Ni) and their Al-substituted compounds, and formation energies calculated from DFT.

	Cu	Ni	Zr	Al
E (Ryd/atom)	-3310.05273	-3041.65413*	-7198.42269	-485.64290
	$CuZr_2$	$Al_{1/4}Cu_{3/4}Zr_2$	$NiZr_2$	$Al_{1/4}Ni_{3/4}Zr_2$
E (Ryd/FU)	-17706.9293	-17000.8259	-17438.5743	-16799.5588
ΔH_f (Ryd/FU)	-0.03119	-0.03020	-0.07479	-0.06207
ΔH_f (eV/FU)	-0.42436	-0.41086	-1.01759	-0.84454
ΔH_f (kJ/mol)	-40.94	-39.64	-98.20	-81.49

*Non-magnetic Ni metal: *E* = -3041.64927 Ryd/atom.

4.2 Electronic structures

From our DFT calculations, all compounds here are found non-magnetic metals. The calculated densities of states (DOS) with contribution of atomic muffin-tin spheres are shown in Fig. 1 and 2. Figs 1(a) and 2(a) show that the lower part of the valence band is dominated by Cu and Ni 3d-states, with broader 3d-bands in the case of $NiZr_2$, due to strong Ni-Ni interactions (1D Ni ion chains). The Zr states contribution rises with energy and becomes dominant at Fermi level. Metal-Zr interactions occur throughout the energy range, with a peak in the lower part of $NiZr_2$ DOS, corresponding to bonding Ni-Zr interactions.

The Al:metal substitution induces a strong perturbation of DOS curves, with the net stabilization of an Al 3s-character band, with bonding metal-Al, Zr-Al interactions (Figs 1(b, c) and 2(b, c)). Thus the overall chemical bonding is strongly affected by the Al:metal substitution. The loss in formation energies with the substitution is the resultant of stabilizing Al(3s)-metal and Al(3s)-Zr bonding interactions, competing with antibonding interactions of same character (3s antibonding bands are partly occupied) and an overall destabilization of the electronic structures in terms of translation symmetry: Al ions involve a different, more ionic chemical bonding than Cu and Ni ions, breaking thus long-range metallic interaction chains.

Table 2 shows the atomic charges deduced from the AIM partitioning of the calculated electron densities. $NiZr_2$ appears as significantly more ionic than $CuZr_2$. **The net negative charge carried by Al ions is only 63% of Cu charge, and 36% of Ni charge, acting thus as a strong perturbation of the Madelung potential in each compound**. Ni ions bonded to Al ions gain a significant charge and lead to the large difference in Al charge between the Cu and Ni compounds. Beyond this effect of short Ni-Al bonds, the differences in crystal structures induce a distribution in Zr charges in $Al_{1/4}Cu_{3/4}Zr_2$, while a single Zr site (and charge) is found in $Al_{1/4}Ni_{3/4}Zr_2$.

Table 2. Net charges calculated by the AIM partitioning of the total electron density.

	Cu/Ni	Zr	Al
$CuZr_2$	-1.08	+0.55	
$Al_{1/4}Cu_{3/4}Zr_2$	-1.08 / -1.11	+0.49 / +0.50 / +0.53	-0.68
$NiZr_2$	-1.31	+0.65	
$Al_{1/4}Ni_{3/4}Zr_2$	-1.48 / -1.30	+0.59	-0.46

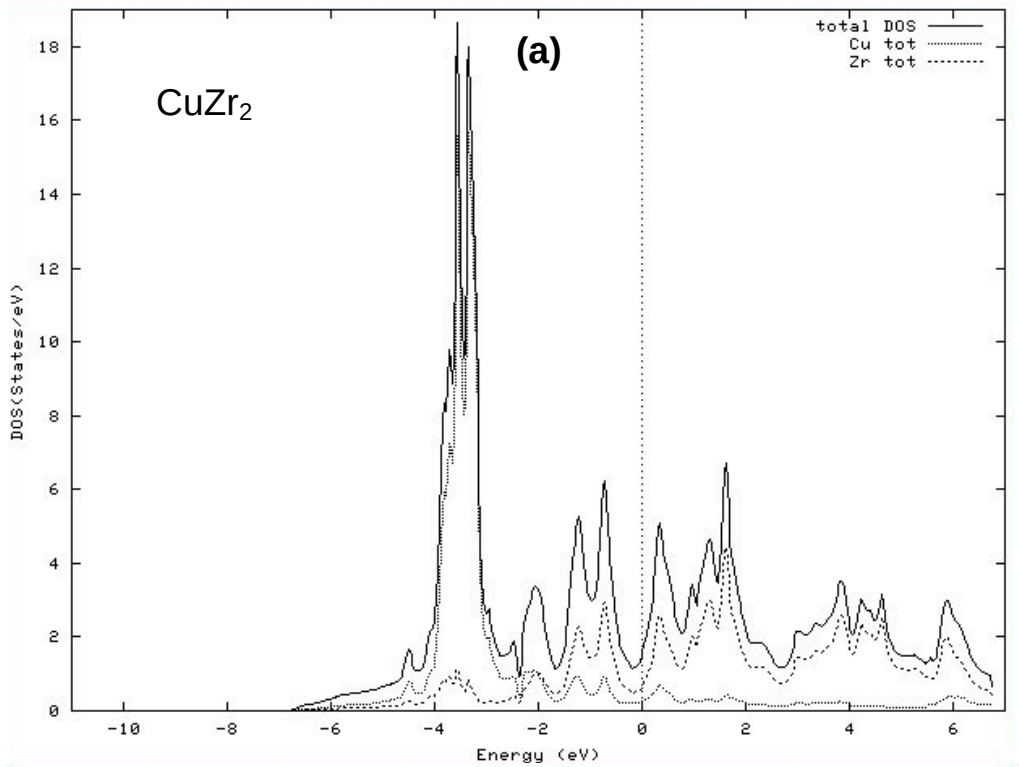
(a)
CuZr2
total DOS
Cu tot
Zr tot
DOS(States/eV)
Energy (eV)

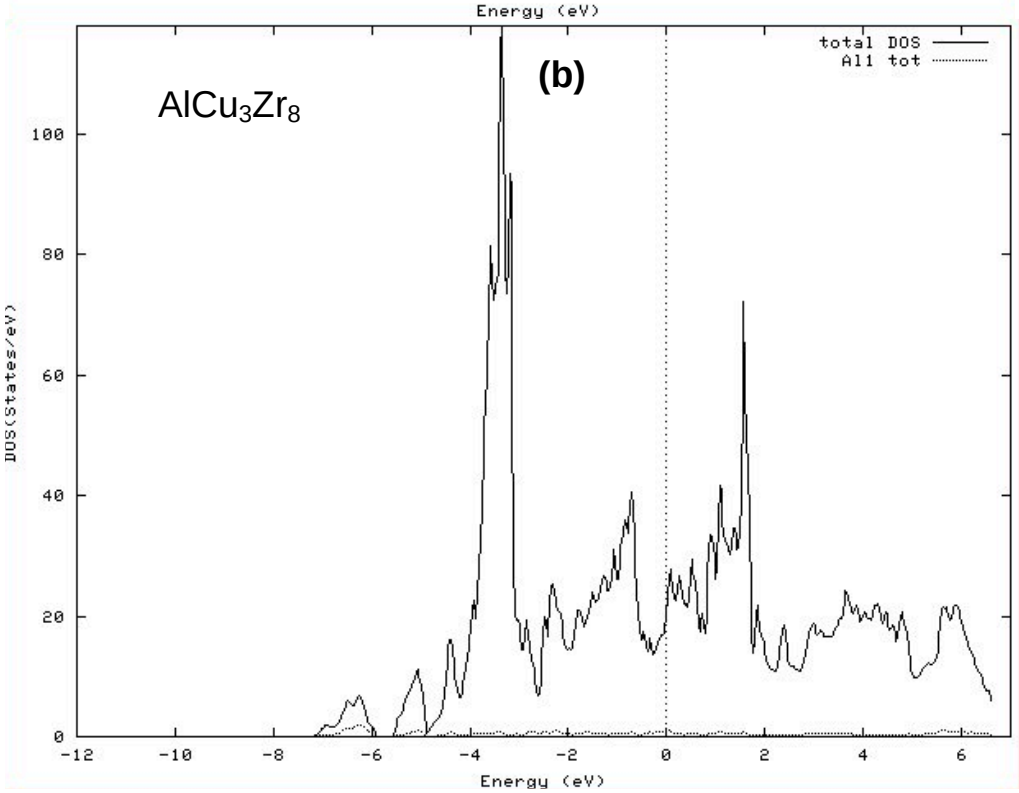
(b)
AlCu3Zr8
total DOS
Al1 tot
DOS(States/eV)
Energy (eV)

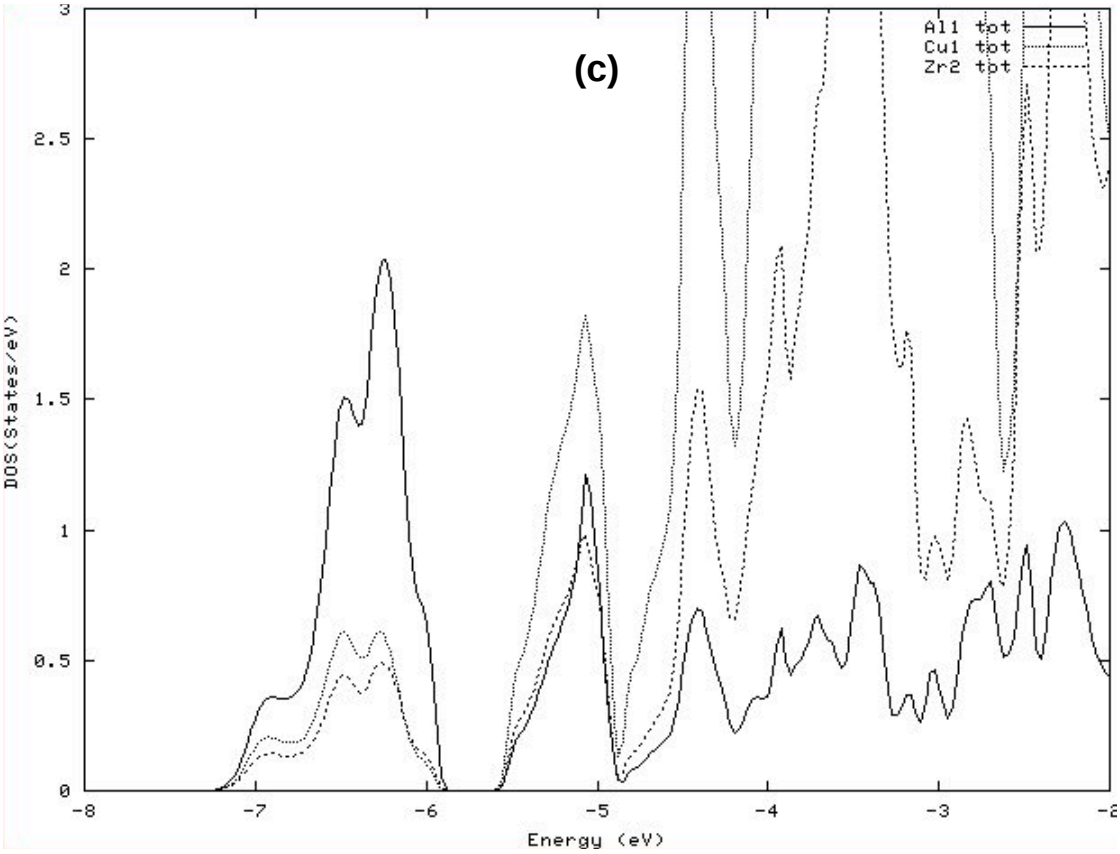

Figure 1. Total and projected DOS for $CuZr_2$ and $Al_{1/4}Cu_{3/4}Zr_2$, calculated by the L/APW+lo DFT method.

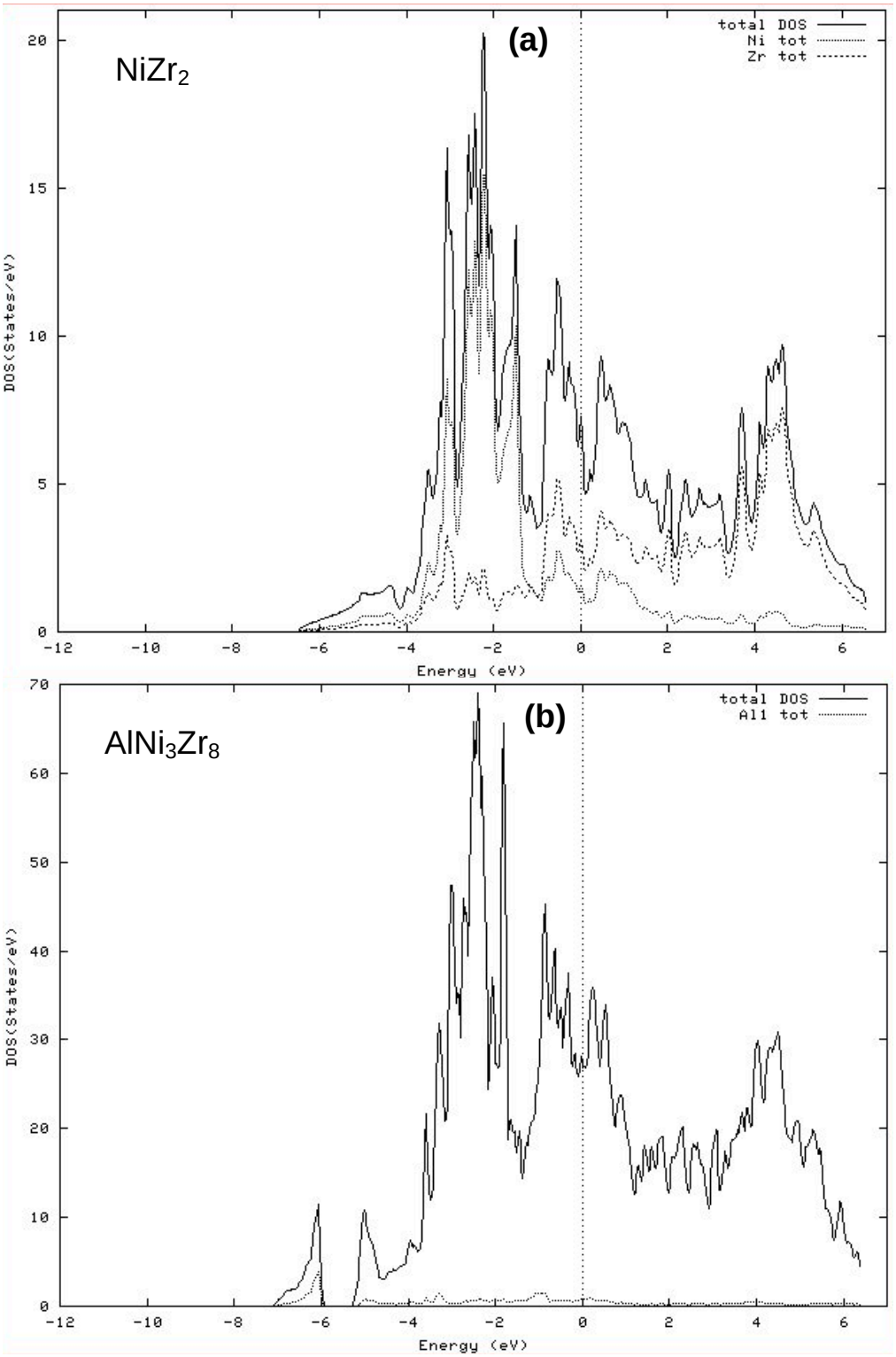
(a)
NiZr2
total DOS
Ni tot
Zr tot
DOS(States/eV)
Energy (eV)
(b)
AlNi3Zr8
total DOS
Al1 tot
DOS(States/eV)
Energy (eV)

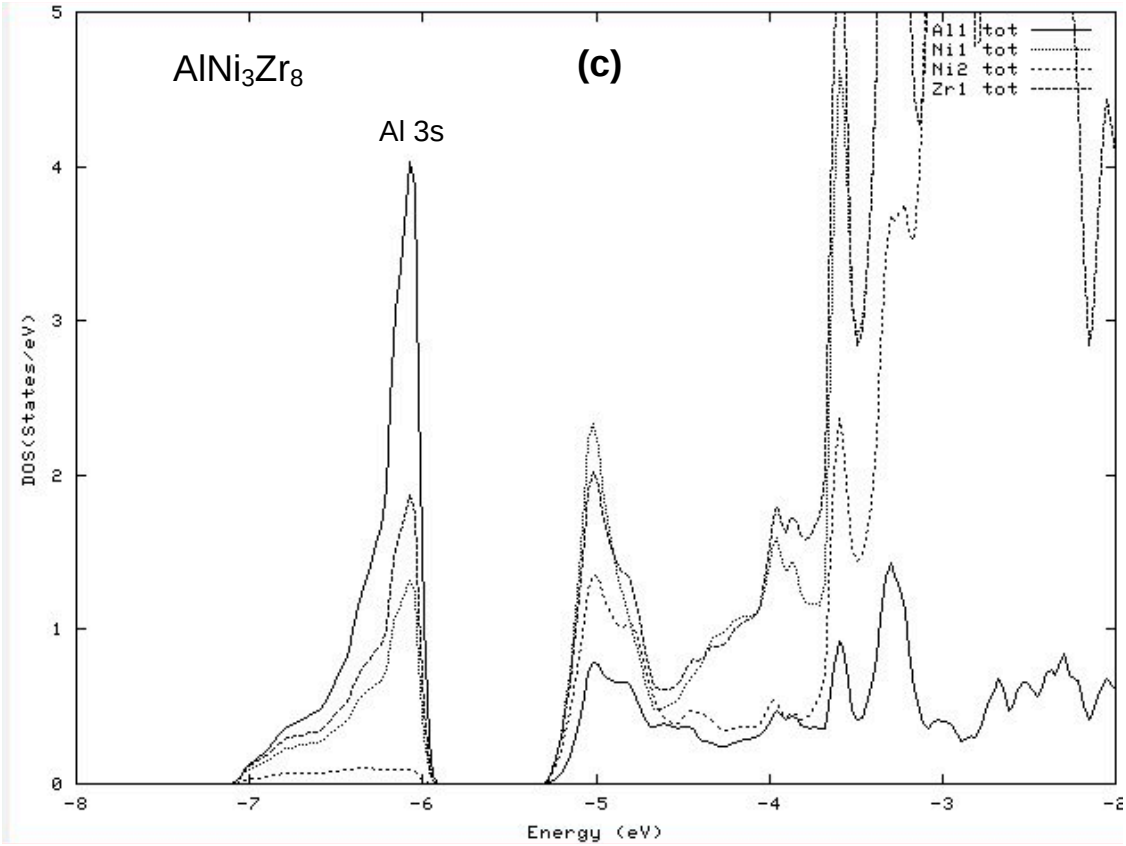

Figure 2. Total and projected DOS for $NiZr_2$ and $Al_{1/4}Ni_{3/4}Zr_2$, calculated by the L/APW+lo DFT method.

4.3 Chemical bonding

The topology of the electron density $\rho(\mathbf{r})$ is characterized by critical points, where the first derivatives of $\rho(\mathbf{r})$ vanish. Thus critical points are maxima (nuclei), minima or saddle points in $\rho(\mathbf{r})$; chemical bonding features are mainly associated to the distribution and characteristics of saddle critical points. A critical point at $\mathbf{r}_c$ can be further characterized by the Hessian eigenvalues of ρ at $\mathbf{r}_c$ (i.e. laplacian of $\rho(\mathbf{r})$ along local principal axes), by its signature (algebraic sum of the signs of the three Hessian eigenvalues), by the ratio $\theta = \lambda_{//} / |\lambda_{\perp}|$ of the laplacian value parallel to the bond path to its main perpendicular component, and by the value of $\rho(\mathbf{r}_c)$ itself.[12,14]

The nature of chemical bonding can be discussed on the basis of critical points characteristics: [14,16]

- Shared interactions (covalent, polar bonding) correspond to $\nabla^2\rho(\mathbf{r}_c) < 0$, $\theta < 1$, large $\rho(\mathbf{r}_c)$,
- Closed-shell interactions (ionic, hydrogen bonding) correspond to $\nabla^2\rho(\mathbf{r}_c) > 0$, $\theta > 1$, relatively low $\rho(\mathbf{r}_c)$,
- Metallic bonding: $\nabla^2\rho(\mathbf{r}_c) > 0$, low $\rho(\mathbf{r}_c)$,
- In general, cohesive energies vary as $\rho(\mathbf{r}_c)$.

These limiting cases and general rules are illustrated in Table 3, where critical points characteristics for diamond (covalent and high cohesive energy) and sodium chloride (archetypal ionic compound) are displayed.

Table 3. Critical points characteristics for diamond and sodium chloride, from the AIM analysis of the calculated electron density. All values are in atomic units (a.u.) $\times 10^4$.

Bond path	Signature	Hessian eigenvalues			Trace	$\rho(\mathbf{r}_c)$
		$\lambda_{//}$	$\lambda_{\perp}$	$\lambda_{\perp}$	$\nabla^2\rho(\mathbf{r}_c)$	
C-C	-1	1168	-4211	-4211	-7254	2387
Na-Cl	-1	752	-89	-89	575	117

Table 4 lists the same characteristics for critical points in elemental metals, as calculated in our study. As expected, values indicate an intermediate situation between covalent and metallic bonding for Cu, Ni and Al; cohesive energies ($\rho(\mathbf{r}_c)$) vary as Ni > Cu > Al (in agreement with tendencies in experimental bulk modulus), correlated to a partial transfer from covalent to metallic bonding in the series (θ , $\nabla^2\rho(\mathbf{r}_c)$).

The case of zirconium metal is more complex, with large θ values and moderate electron density at critical points, a situation with closed-shell (ionic cores) and metallic interactions. The main type of critical points (Zr-Zr 1st neighbors) as a unusual +1 signature, and critical points are found for 2nd and 3rd neighbors too, indicating a complex or diffuse (metallic?) chemical bonding picture.

Table 4. Critical points characteristics for elemental metals, from the AIM analysis of the calculated electron density. All values are in a.u. $\times 10^4$.

Bond path	Signature	Hessian eigenvalues			Trace	
		$\lambda_{//}$	$\lambda_{\perp}$	$\lambda_{\perp}$	$\nabla^2\rho(\mathbf{r}_c)$	
Cu-Cu	-1	164	-161	-109	-106	391
Ni-Ni	-1	108	-199	-136	-226	462
Al-Al	-1	109	-103	-28	-22	299
Zr-Zr	+1	292	35	-52	274	257
2nd neigh.	-1	150	-57	-48	44	294
3rd neigh.	+1	12	12	-7.5	17	202

Some tendencies of elemental metals are retrieved in the critical points of the calculated electron density for $CuZr_2$, $Al_{1/4}Cu_{3/4}Zr_2$ (Table 5), $NiZr_2$ and $Al_{1/4}Ni_{3/4}Zr_2$ (Table 6). Ni-Ni interactions are stronger than Cu-Cu, and Zr-Zr bonding remains complex with +1 signatures and long-range interactions. All traces are positive, indicating competing interactions as found in iono-covalent and metallic compounds.

Ni 1D chains in $NiZr_2$ contain shared-interactions critical points, similarly to Ni metal. This participates to the large stability of $NiZr_2$, despite the lower dimensionality of Ni-Ni

interactions than in the metal. The overall $\rho(\mathbf{r}_c)$ values are larger in $NiZr_2$ than in $CuZr_2$, in agreement with the larger formation energy of the former.

Cu-Zr interactions dominate in $CuZr_2$ and the Cu-Cu bonding is weaker than in Cu metal; the crystal structure plays an important role here, but might be seen itself as a consequence of weaker Cu-Cu bonding compared to Ni-Ni. $\nabla^2\rho(\mathbf{r}_c)$ and $\rho(\mathbf{r}_c)$ values in Tables 5 and 6 show that positively charged Zr ions (Table 2) form stronger Zr-Zr bonds than in Zr elemental metal.

As seen in Tables 5 and 6, Al:Cu and Al:Ni substitutions induce a narrow but significant distribution of Hessian eigenvalues and $\rho(\mathbf{r}_c)$ values, indicating a perturbed chemical bonding distribution in the two compounds. Critical points for Zr-Zr interactions appear, that were not present in the parent compounds, showing thus a higher degree of competition between interactions in the Al-substituted systems.

Furthermore, a strong perturbation of the crystals bonding schemes is induced by the very different nature of Al-metal bonds, compared to the parent interactions involving Cu and Ni. This appears clearly too in the electron density maps shown in Figures 3 and 4.

A point that remains unclear is the absence of Ni-Ni and Ni-Al critical points for $Al_{1/4}Ni_{3/4}Zr_2$ (Table 6), whereas the strong 1D interactions found in $NiZr_2$ still exist. This is a numerical artifact still to be resolved.

From Tables 5 and 6, the perturbations induced by the Al substitution appear more numerous in $CuZr_2$ than in $NiZr_2$; however, the values distribution is somewhat broader in $Al_{1/4}Ni_{3/4}Zr_2$, and bond paths slightly larger than bond lengths in this system indicate too an instability in the crystal structure. The chemical bonding, critical points nature and distribution are strongly perturbed and disordered in both compounds by the Al:metal partial substitution; this might strongly influence the tendency to glassy transition, together with the global stability of the parent crystalline systems and the non trivial features of Zr-Zr bonding. On the other side, Ni-Ni bonding appears to be both strong and directional, even in binary or ternary systems; this may be an unfavorable factor for a glassy transition.

Table 5. Critical points characteristics for $CuZr_2$ (top) and $Al_{1/4}Cu_{3/4}Zr_2$ (bottom), from the AIM analysis of the electron density. All values are in a.u. $\times 10^4$ except path lengths (Å).

Bond path	Path length	Signature	Hessian eigenvalues			Trace	$\rho(\mathbf{r}_c)$
			$\lambda_{//}$	$\lambda_\perp$	$\lambda_\perp$	$\nabla^2\rho(\mathbf{r}_c)$	
Cu-Zr	2.85	-1	402	-120	-118	165	322
Cu-Cu	3.22	-1	271	-42	-40	189	246
Zr-Zr	3.14	+1	296	63	-67	292	281
Cu1-Zr	2.85	-1	399	-105	-116	178	320
		-1	401	-105	-116	179	320
		-1	398	-106	-119	173	322
		-1	399	-107	-116	177	321
Cu2-Zr	2.85	-1	404	-117	-121	166	323
		-1	401	-118	-123	160	324
		-1	403	-117	-120	166	322
Al-Zr	**2.85**	**-1**	**276**	**-80**	**-86**	**110**	**332**
		-1	**278**	**-80**	**-83**	**115**	**330**
		-1	**280**	**-82**	**-83**	**115**	**331**
Cu1-Cu2	3.22	-1	270	-42	-40	188	246
Al-Cu1	**3.22**	**-1**	**207**	**-48**	**-46**	**113**	**275**
		-1	**208**	**-49**	**-46**	**113**	**274**
Zr-Zr	3.14	+1	300	70	-76	294	281
		+1	297	67	-72	292	280
		+1	302	64	-73	293	281
		+1	296	68	-66	298	278
		+1	304	57	-73	288	282
Zr-Zr	**3.38**	**+1**	**156**	**85**	**-33**	**207**	**251**
		+1	**153**	**85**	**-35**	**203**	**253**
Zr-Zr	**3.45**	**+1**	**128**	**113**	**-25**	**215**	**230**
		+1	**130**	**113**	**-25**	**218**	**230**

Table 6. Critical points characteristics for $NiZr_2$ (top) and $Al_{1/4}Ni_{3/4}Zr_2$ (bottom), from the AIM analysis of the electron density. All values are in a.u. $\times 10^4$ except path lengths (Å).

Bond path	Path length	Signature	Hessian eigenvalues			Trace	$\rho(\mathbf{r}_c)$
			$\lambda_{//}$	$\lambda_{\perp}$	$\lambda_{\perp}$	$\nabla^2\rho(\mathbf{r}_c)$	
Ni-Zr	2.76	-1	390	-137	-143	109	384
Ni-Ni	2.63	-3	-121	-121	-8	-251	430
Zr-Zr	2.99	-1	486	-43	-36	407	291
Zr-Zr	3.08	+1	398	30	-19	409	255
	3.56	+1	128	25	-16	137	225
Ni1-Zr	2.76	-1	386	-141	-132	112	390
	2.77	**-1**	**401**	**-137**	**-133**	**131**	**378**
Ni2-Zr	2.77	-1	397	-144	-137	113	382
Al-Zr	**2.80**	**-1**	**274**	**-125**	**-85**	**64**	**387**
Zr-Zr	2.99	-1	486	-44	-33	410	286
Zr-Zr	3.08	+1	398	24	-19	402	255
	3.13	**+1**	**327**	**70**	**-31**	**365**	**264**
	3.38	**+1**	**197**	**21**	**-17**	**201**	**240**
	3.38	**+1**	**201**	**9**	**-21**	**189**	**242**
	3.56	+1	121	29	-13	137	223
	3.75	**+1**	**88**	**37**	**-13**	**111**	**234**

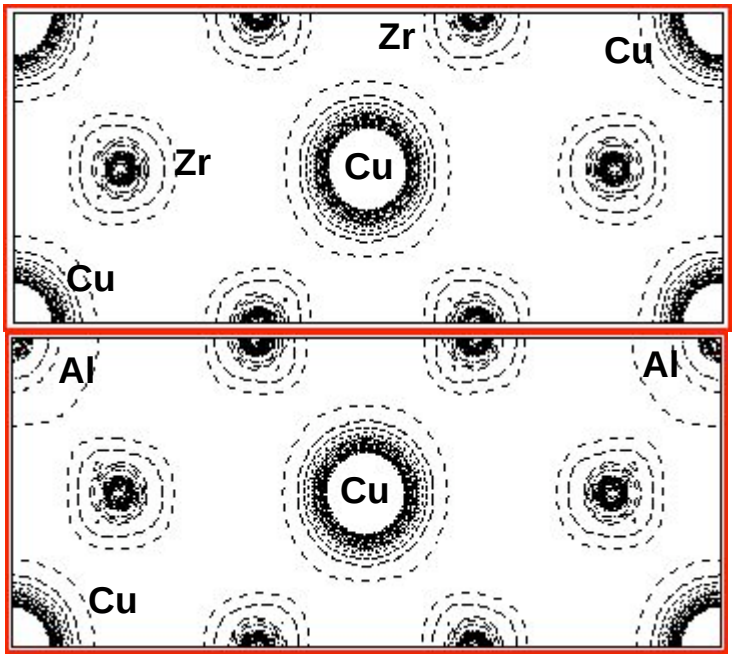

Figure 3. Electron density map for $CuZr_2$ (top) and $Al_{1/4}Cu_{3/4}Zr_2$ (bottom), calculated with the L/APW+lo DFT method.

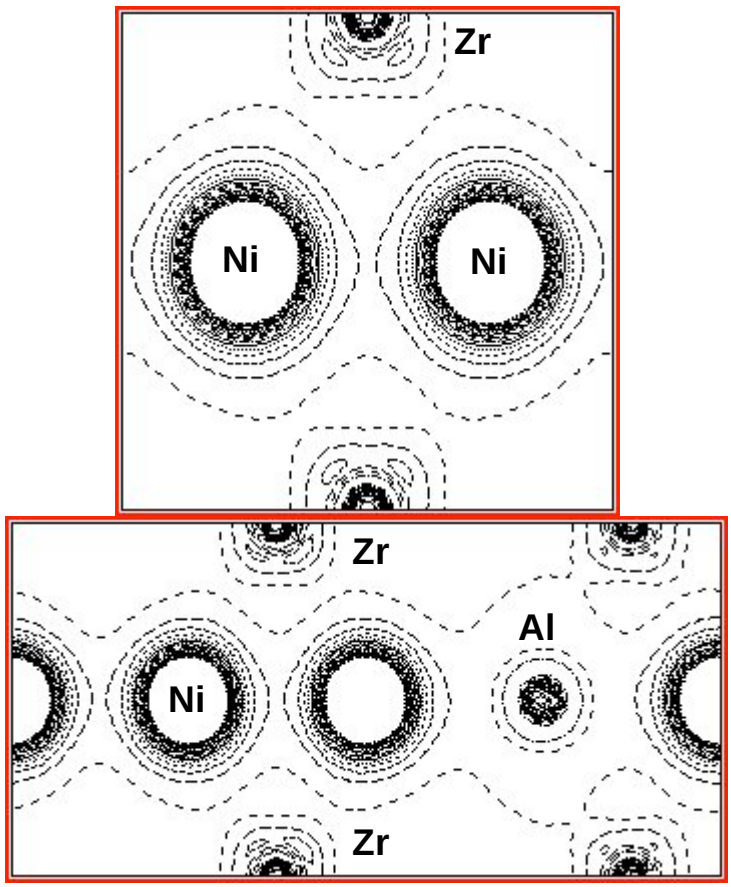

Figure 4. Electron density map for $NiZr_2$ (top) and $Al_{1/4}Ni_{3/4}Zr_2$ (bottom), calculated with the L/APW+lo DFT method.

5. Conclusion

The role of chemistry on the enhancement of the formation of glassy phase in binary Cu-Zr and Ni-Zr alloys by Al substitution was carried out by analysis of the electronic structure, chemical bonding, nature and distribution of critical points of the electron density in Cu-Zr, Ni-Zr, Al-Cu-Zr and Al-Ni-Zr compounds with compositions within the glass forming range.

It was found that the overall chemical bonding is strongly affected by Al:metal partial substitution through the following features:

- Al ions carry a much lower net charge than Cu and Ni ions, and break the site equivalencies for the net charges of Cu, Ni and, in the case of $NiZr_2$, Zr. Therefore, the electrostatic field at each site (Madelung potential) is strongly perturbed and has a lower symmetry.
- Al-metal bonding involves Al 3s orbitals, that have a different symmetry and extent than Cu and Ni 3d orbitals. Thus Al ions break metal interaction chains and related energy dispersion (bands) and destabilize the host crystal lattices. Strong Ni-Ni bonds are specifically affected, leading to a significant loss in formation energy for Al:$NiZr_2$.
- The distribution of critical points in the electron density is strongly affected by the Al:metal substitution; the chemical bonding patterns become more complex, with an increase of next-nearest neighbors interactions for Zr-Zr bonds. The crystal structure is under strain due to competing interactions and symmetry lowering.

These results suggest that the enhancement of the formation of the glassy phase by Al substitution in these systems has a strong chemical origin and can be attributed to the destabilization and perturbation of the bonding pattern of the crystal structure.

Trends found in this study should be transferable to other crystal/glass compositions in this family. More general results concern the strength and directionality of Ni-Ni bonding, and the transformation of the covalent character of bonding in elemental metals into a much more iono-covalent character in binary compounds. The agreement between calculated and experimental formation energies, and trends in cohesive energies for elemental metals, make this approach promising and reliable for further stability and glass formation studies.

References

(1) A. Inoue, Mat. Sci. Eng. A226-228 (1997) p. 357.

(2) D.B. Miracle, Nature Materials 3 (2004) p. 697.

(3) D.B. Miracle, Acta Mater. 54 (2006) p. 4317.

(4) J.-Z. Yu, A.-P. Tsai and T. Masumoto, "Nonequilibrium Phase Diagrams of Ternary Amorphous Alloys" in Phase Diagrams and Physical Properties of Nonequilibrium Alloys, (Y. Kawazoe, eds.) Vol. 37A Springer-Verlag Berlin, Germany (1997).

(5) Zhang, Inoue and Matsumoto, Trans. JIM (1991) p. 1005.

(6) Sviridova, T. A.; Diakonova, N. P.; Shelekhov, E. V.; Glazkov, V. P. *Poverkhnostnye Fizika, Khimiya, Mekhanika* 2004, **10**, 28. FIZ Karlsruhe: Inorganic Crystal Structure Database #151846.

(7) Havinga, E. E.; Damsma, H.; Hokkeling, P. *J. Less Common Met.* 1972, **27**, 169. FIZ Karlsruhe: Inorganic Crystal Structure Database #102805.

(8) Blaha, P.; Schwarz, K.; Madsen, G. K. H.; Kvasnicka, D.; Luitz, J. *WIEN2k, An Augmented Plane Wave Plus Local Orbitals Program for Calculating Crystal Properties*; Vienna University of Technology: Vienna, Austria, 2001.

(9) Sjöstedt, E.; Nordström, L.; Singh, D. *Solid State Commun.* 2000, **114**, 15.

(10) Madsen, G. K. H.; Blaha, P.; Schwarz, K.; Sjöstedt, E.; Nordström, L. *Phys. Rev. B* 2001, **64**, 195134.

(11) Perdew, J. P.; Burke, K.; Ernzerhof, M. *Phys. Rev. Lett.* 1996, **77**, 3865.

(12) Bader, R. F. W.; Essen, H. *J. Chem. Phys.*, 1984, **80**, 1943.

(13) Bader, R. F. W. *Chem. Rev.*, 1991, **91**, 893.

(14) Bader, R. F. W. *Atoms in Molecules : A Quantum Theory*; Clarenden Press: Oxford, 1994.

(15) Bader, R. F. W. *J. Phys. Chem. A*, 1998, **102**, 7314.

(16) Na Wang; Changrong Li; Zhenmin Du; Fuming Wang, Weijing Zhang *Calphad* 2006, **30**, 461.

(17) Na Wang; Changrong Li; Zhenmin Du; Fenge Wang *Calphad* 2007, **31**, 413.